Feasibility of the Estimation of Myocardial Stiffness with Reduced 2D Deformation Data

Anastasia Nasopoulou[1] (✉), David A. Nordsletten[1], Steven A. Niederer[1], and Pablo Lamata[1]

Department of Biomedical Engineering, Division of Imaging Sciences and Biomedical Engineering, King's College London, London, UK
anastasia.nasopoulou@kcl.ac.uk

Abstract. Myocardial stiffness is a useful diagnostic and prognostic biomarker, but only accessible through indirect surrogates. Computational 3D cardiac models, through the process of personalization, can estimate the material parameters of the ventricles, allowing the estimation of stiffness and potentially improving clinical decisions. The availability of detailed 3D cardiac imaging data, which are not routinely available for the conventional cardiologist, is nevertheless required to constrain these models and extract a unique set of parameters. In this work we propose a strategy to provide the same ability to identify the material parameters, but from 2D observations that are obtainable in the clinic (echocardiography). The solution combines the adaptation of an energy-based cost function, and the estimation of the out of plane deformation based on an incompressibility assumption. In-silico results, with an analysis of the sensitivity to errors in the deformation, fibre orientation, and pressure data, demonstrate the feasibility of the approach.

Keywords: Cardiac mechanics · Myocardial stiffness · Energy-based cost function · Parameter estimation · 2D images

1 Introduction

Left ventricular (LV) stiffness has been identified as a useful biomarker in the diagnosis and monitoring of heart failure (HF) with preserved ejection fraction, a syndrome which is associated with high morbidity and mortality rates and poor prognosis [1, 2]. The assessment of myocardial stiffness in vivo is a complex task which can be tackled with the use of cardiac biomechanical models. In these models material stiffness is determined from the choice of parameter values in the employed material constitutive equations, and therefore the problem of stiffness estimation is posed as a parameter estimation problem. A major limitation in this approach is the parameter coupling in common material models [3], resulting in multiple parameter combinations corresponding to equivalent solutions in the optimization. This inability to uniquely constrain parameters limits the correlation of changes in material parameters to possible changes in patient pathophysiology. The problem of parameter coupling was recently addressed by

a novel energy-based cost function (CF), which was applied to detailed 3D geometry and deformation data available from magnetic resonance imaging (MRI) [4].

However, MRI scanners are expensive and scarce and the reliance of parameter estimation pipelines on the availability of 3D data limits their possible impact in the large scale. Conversely, planar ultrasound images are ubiquitous in clinical practice. Aiming to translate the recent advances in parameter estimation from 3D clinical models into the clinic and the constraints of everyday practice, this paper investigates the possibility to assess myocardial parameters from 2D geometry data, such as would be available from long axis echocardiographic views of the LV.

2 Materials and Methods

Parameter estimation in this study relies on recent work [4] where a CF was proposed based on the energy conservation of the myocardium during diastolic filling. This CF solves the problem of coupling between the scaling and bulk exponential parameters in material models and was applied on a popular transversely isotropic model proposed by Guccione et al. [5].

To investigate the feasibility of myocardial stiffness estimation, a synthetic data set was generated in order to provide ground truth (GT) solutions to material parameters and knowledge of 'real' 3D deformations (Section 2.2). The information from this model was subsequently modified in order to serve two scenarios. In the first, geometrical information is available on a 2D plane only, but the full 3D displacements and displacement gradients of the material points on this plane are assumed to be known. In the second, only 2D information on LV geometry and deformation is available. To assess the effect of data noise and certain material modelling assumptions, a sensitivity study was performed highlighting the robustness of each of the two cases of data availability (Section 2.3).

A new version of the energy-based CF [4] is introduced in this study for the estimation of the exponential parameter, and the different strategies employed for the CF evaluation depending on the available data set are explained in Section 2.5. In the last paragraph of this section, we complete the parameter estimation by presenting a method to estimate the remaining coupled scaling parameter (Section 2.6).

2.1 Material Model

The myocardium was modelled as a transversely isotropic material [5] with a strain energy density function (Eqs. (1),(2)) expressed as a function of a scaling parameter (C_1) and a bulk exponential parameter (α) [6]. The parameters r_f,r_t,r_{ft} scale the Green-Lagrange strain tensor ($\boldsymbol{E}$), where $\boldsymbol{E}$ is expressed in fiber coordinates. The subscripts f,s,n denote the tensor components in the fiber, sheet and sheet normal directions. The fiber orientation in the LV myocardial

wall was assumed to follow an idealised $-60°/+60°$ distribution from the epi- to the endocardium [7].

$$\Psi = \frac{1}{2}C_1(\mathrm{e}^Q - 1) \tag{1}$$

$$\begin{aligned} Q =& \alpha[r_f {E_{ff}}^2 + r_{ft}({E_{fs}}^2 + {E_{sf}}^2 + {E_{fn}}^2 + {E_{nf}}^2) \\ &+ r_t({E_{ss}}^2 + {E_{nn}}^2 + {E_{sn}}^2 + {E_{ns}}^2)] \end{aligned} \tag{2}$$

As the main direction of coupling in the Guccione law is along C_1 and α, which scale stiffness along all directions [6], in this study we focus on C_1-α estimation and assume the anisotropy parameters are fixed (see Section 2.2 for the chosen GT values), following a common approach [4, 8].

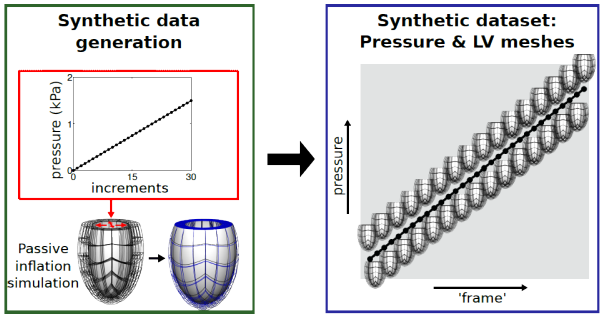

Fig. 1. Passive inflation simulation of a prolate spheroidal finite element (FE) model of the LV to generate the original pressure - 3D geometry data.

2.2 Ground Truth: 3D in Silico Model

For the generation of the 3D GT data set, from which the synthetic 2D 'images' will be derived, the left ventricle (LV) was modelled as a truncated ellipsoid of revolution of human dimensions. It was passively inflated to 1500 Pa end diastolic pressure under fully constrained basal displacements to generate the original pressure - 3D geometry data. The constructed finite element (FE) mesh consisted of 320 elements (4 circumferential, 4 transmural, 4 longitudinal and 16 in the apical cap) and 9685 nodes. The pressure was applied in 30 increments of 50 Pa each and basal plane was fixed by prescibing the Dirichlet boundary conditions directly at the basal nodes of the mesh.

The deformation was found by solving the linearised total potential energy equations using the *CHeart* nonlinear mechanics solver [9], using a split $\boldsymbol{u}$-p formulation outlined in [10]. The initial geometry ($\boldsymbol{X}$), deformed geometry ($\boldsymbol{x}$) and fiber orientation ($\boldsymbol{f}, \boldsymbol{s}, \boldsymbol{n}$) vector fields were interpolated through cubic-Lagrange

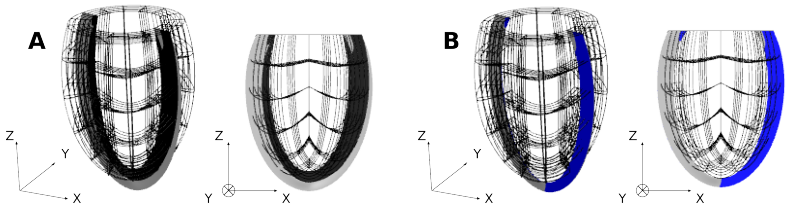

Fig. 2. Synthetic 'images' for the 3D simulations (Fig. 1). **A**. Data set 1 (3D deformation information): undeformed geometry is the slice in black and deformed geometry is shown in grey, where a small twist can be observed. **B**. Data set 2 (2D deformation information): the 'real' deformed geometry (used in data set 1) is shown in grey as in panel A, and in blue is the geometry resulting from the projection of the 'real' deformation on the XZ plane (this is used in data set 2) - note that the twist is now removed. The mesh in both panels corresponds to the original 3D undeformed geometry.

shape functions. To avoid locking phenomena, the 'hydrostatic pressure' field (p) approximation needs to be of a lower order [11], and in this case a Linear-Lagrange interpolation scheme was used for computational economy (reduction of stiffness matrix size and use of the already available linear mesh). The meshes and simulation outputs were visualised with *cmGui* [1].

The Guccione material parameters chosen for the generation of the synthetic data set were: $C_1 = 1000Pa$, $\alpha = 30$, $r_f = 0.55$, $r_{ft} = 0.25$ and $r_t = 0.2$ [4]. For clarifying aspects regarding the severity of errors in the identified parameters as well as aspects of the sensitivity analysis, two additional 3D GT data sets were generated (see also last two rows of Table 2), one with C_1= 300, α=100, r_f=0.55, r_{ft}=0.25, r_t=0.2 and another with C_1=1000 Pa, α=30, r_f=0.85, r_{ft}=0.1, r_t=0.05 (the remaining aspects of the data set being identical).

2.3 Synthetic Data Sets from in Silico Model and Corresponding Modelling Approaches

Case 1: Synthetic Data Set of 2D LV Geometry - 3D Deformation. The first data set that will be examined consists of cavity pressure measurements and geometry and 3D deformation of a long axis plane of the myocardium across 31 'frames' corresponding to the simulation increments (reference mesh and 30 simulation outputs) of the initial 3D synthetic data set (Section 2.2). In this case the long axis plane was chosen to 'cut' the existing 3D mesh into 2 symmetric halves and coincides with the XZ plane in the undeformed configuration (see Fig. 2).

Case 2: Synthetic Data Set of 2D LV Geometry - 2D Deformation. The second case of the synthetic data set consists of the pressure measurements, 2D

[1] http://www.cmiss.org/cmgui

geometry and 2D deformation across the 31 'frames' from the original simulation (Section 2.2). The synthetic 'image' of the LV is again in the XZ plane as in the first case. The difference here is that only 2D information of the deformation field is provided (Eqs. 3) , which is achieved by projecting the 'real' deformation field into the 'imaging' plane (XZ) (see Fig. 2).

The estimation of the energy-based CF in Section 2.5 requires the estimation of the Green-Lagrange strain tensor in the 3D fiber coordinate system (Eq. (2)), which in turn requires the description of deformation in three dimensions. In the case of the limited, in-plane deformation data this requires an assumption to be made about the off-plane deformation patterns. For this purpose, two different approaches were followed. In the first, plane strain is assumed and the 3D displacement and deformation gradient are taken as $\boldsymbol{u}_{3D}$ and $\boldsymbol{F}_{p.s.}$ in Eq. (4). In the second, the off-plane shear is again assumed to be zero but the term $\frac{\partial y}{\partial Y}$ is estimated from the isovolumic deformation assumption for the myocardium (the 3D description of the displacement is again $\boldsymbol{u}_{3D}$ but the deformation gradient is now $\boldsymbol{F}_{iso}$ in Eq. (4)).

$$\boldsymbol{u}_{2D} = \begin{bmatrix} u_x \\ u_z \end{bmatrix} \ , \ \boldsymbol{F}_{2D} = \begin{bmatrix} \frac{\partial x}{\partial X} & \frac{\partial x}{\partial Z} \\ \frac{\partial z}{\partial X} & \frac{\partial z}{\partial Z} \end{bmatrix} \tag{3}$$

$$\boldsymbol{u}_{3D} = \begin{bmatrix} u_x \\ 0 \\ u_z \end{bmatrix} \ , \ \boldsymbol{F}_{p.s.} = \begin{bmatrix} \frac{\partial x}{\partial X} & 0 & \frac{\partial x}{\partial Z} \\ 0 & 1 & 0 \\ \frac{\partial z}{\partial X} & 0 & \frac{\partial z}{\partial Z} \end{bmatrix} \ , \ \boldsymbol{F}_{iso} = \begin{bmatrix} \frac{\partial x}{\partial X} & 0 & \frac{\partial x}{\partial Z} \\ 0 & \frac{1}{det(\boldsymbol{F}_{2D})} & 0 \\ \frac{\partial z}{\partial X} & 0 & \frac{\partial z}{\partial Z} \end{bmatrix} \tag{4}$$

2.4 Evaluation of Performance

Sensitivity Study. To provide an estimation of the severity of data quality and model-data discrepancies on the estimated parameter values in 2D, a sensitivity study was performed. For estimating effects of miscalibration in pressure measurements, synthetic data sets with modified pressure traces (pressure offset by $\pm 10\%$ of mean pressure value) were used. To examine the effect of the imaging data on the accuracy of the analysis two additional data sets were used, where white Gaussian noise was inserted to the deformation field. Specifically, for each component of the deformation gradient F_{ij} $(i, j = 1, \ldots, N$, where $N = 9$ for the 3D deformation data set and $N = 4$ for the 2D) its mean value ($\bar{F}_{ij}$) over the Gauss points (GPs) of the in-plane surface mesh elements was estimated (432 GPs used in total, equivalent to 3 GPs used per element direction). A normal distribution of random numbers was generated (independently for each frame and F_{ij}), was weighted by either 1% or 2% of $\bar{F}_{ij}$ and subsequently added to each GP of the mesh at each frame generating two sets of noisy deformation data used instead of the 1^{st} and 2^{nd} data sets of Sec. 2.3.

Displacement Errors and Stress-Strain Curves The insilico tests will report the estimated parameters (α and C_1), together with an analysis of the

impact of the error in these parameters with regard to two aspects: (1) the difference in the displacements (L^2 displacement norm), and (2) the difference in the stress-strain relationship in a simple fibre-stretch model. Specifically, forward simulations on the original 3D mesh (Sec. 2.2) were performed using the identified parameters and the resulting L^2 displacement norm ($|\Delta \boldsymbol{u}|$), comparing the deformed geometry of the simulation with the identified parameters and the GT, was estimated [4]. The stress-strain plots refer to an idealised scenario of stretch along the fiber direction of an incompressible cube with the specified α-C_1 parameters. They show the Cauchy stress along the fiber direction (σ_f) minus the indeterminate 'hydrostatic pressure' p term (see Sec. 2.5), in the absence of specified boundary conditions, with respect to fiber stretch (λ_f) (Fig. 3).

To contextualise this analysis, two additional sets of $C_1 - \alpha$ parameters are selected which lie on the $C_1 - \alpha$ principal parameter coupling line at ± 20 of the GT α value (α_{GT}). This line represents parameter combinations that effectively reproduce the same deformation in a model. In our analysis the coupling line was obtained from an exponential fit to the parameter combinations that minimize the $|\Delta \boldsymbol{u}|$ residual (following parameter sweeps over C_1 and α on the original 3D simulation, see Sec. 2.2) and agreed well with the proposed coupling direction by [6] using the mean value of Q (Fig. 3).

2.5 Estimation of the Exponential Parameter α from the Reformulated Energy-Based CF

This study is based on previous work [4], where unique parameter estimation was achieved with the use of an energy-based CF that allowed determination of the α parameter in Eq. (2). This CF was based on energy conservation, dictating that the work of internal stresses inside the tissue stored as elastic energy (W_{int}) and the external work of cavity pressure (W_{ext}) are equal.

Here we re-formulate the energy-based CF based on the principle of virtual work, which expresses the linearisation of the energy balance with respect to an arbitrary displacement field $\delta \boldsymbol{u}$, called the virtual displacement field. Assuming quasi-static loading and absence of residual active tension in the diastolic window of relevance allows the internal (δW_{int}) and external (δW_{ext}) components of the virtual work to be expressed as in Eqs (5) and (6) respectively. In Eq. (5), Ψ is given by (1), and p, J and $\boldsymbol{C}$ denote the 'hydrostatic pressure', the determinant of the deformation gradient and the right Cauchy Green tensor respectively. Eq. (6) is based on a pull-back expression of δW_{ext} based on Nanson's formula [12], where p_C, $\mathrm{d}\boldsymbol{A}$, $\delta \boldsymbol{u}$, $\boldsymbol{F}$ denote the cavity pressure, infinitesimal area vector in the material configuration, virtual displacement, and deformation gradient. The terms $\frac{\partial \Psi}{\partial \boldsymbol{E}}$ and $D\boldsymbol{E}[\delta \boldsymbol{u}]$ are given by Eqs. (7), (8) and (9) [6, 12]. The virtual displacement field in these equations can be arbitrary provided that the boundary conditions of the problem are respected. Here we have employed a virtual field equal to the measured displacements from the data.

Note that although we refer to p as the tissue 'hydrostatic pressure', it is not equal to $1/3tr(\boldsymbol{\sigma})$ due to the non use of the distortional formulation of Ψ ($\hat{\Psi}$),

see [12]. The estimation of p from the data is not neccessary, as the contribution of the term $pJ\boldsymbol{C}^{-1}$ on the virtual work is zero (see Eq. (10) and [12] for the derivation), as long as the virtual displacement field employed respects the incompressibility constraint (so that $DJ[\delta\boldsymbol{u}]$=0). The latter holds in our approach, since the virtual displacements used are equal to the real (incompressible) ones (see Sec. 2.2).

$$\delta W_{int} = \int_V \left(\frac{\partial \Psi}{\partial \boldsymbol{E}} + pJ\boldsymbol{C}^{-1} \right) : D\boldsymbol{E}[\delta\boldsymbol{u}] dV. \tag{5}$$

$$\delta W_{ext} = \int_A p_C J \delta\boldsymbol{u} \cdot \left(\boldsymbol{F}^{-T} d\boldsymbol{A} \right) \tag{6}$$

$$\frac{\partial \Psi}{\partial \boldsymbol{E}} = C_1 \alpha \mathrm{e}^Q \begin{bmatrix} r_f & r_{ft} & r_{ft} \\ r_{ft} & r_t & r_t \\ r_{ft} & r_t & r_t \end{bmatrix} \circ \begin{bmatrix} E_{ff} & E_{fs} & E_{fn} \\ E_{sf} & E_{ss} & E_{sn} \\ E_{nf} & E_{ns} & E_{nn} \end{bmatrix} \tag{7}$$

$$D\boldsymbol{E}[\delta\boldsymbol{u}] = \frac{1}{2} \left(D\boldsymbol{F}[\delta\boldsymbol{u}]^T \boldsymbol{F} + \boldsymbol{F}^T D\boldsymbol{F}[\delta\boldsymbol{u}] \right) \tag{8}$$

$$D\boldsymbol{F}[\delta\boldsymbol{u}] = \boldsymbol{\nabla}\delta\boldsymbol{u}\boldsymbol{F} \tag{9}$$

$$pJ\boldsymbol{C}^{-1} : D\boldsymbol{E}[\delta\boldsymbol{u}] = pJtr\left(\boldsymbol{\nabla}\delta\boldsymbol{u}\right) = pDJ[\delta\boldsymbol{u}] \tag{10}$$

Expressing the principle of virtual work over two diastolic frames 1 and 2, the modified energy-based CF can then be expressed as in Eq. (11). Since both the numerator and denominator of the δW_{int} ratio in Eq. (11) contain the parameter C_1, it is evident that it cancels out and thus f allows for the unique estimation of α. As the α parameter in Eq. (11) lies within e^Q only, (the product $C_1\alpha$ in $\frac{\partial \Psi}{\partial \boldsymbol{E}}$ cancels out), the use of higher strains increases the nonlinearity of the CF and therefore its identifiability. For this purpose the two last 'frames' of the synthetic data set (Frames 29 and 30, corresponding to the last two simulation increments of Sec. 2.2) were chosen as diastolic frames 1 and 2 respectively.

$$f = \left| \frac{\delta W^1_{ext}}{\delta W^2_{ext}} - \frac{\delta W^1_{int}}{\delta W^2_{int}} \right| \tag{11}$$

2.6 Estimation of the Scaling Parameter C_1

To complete the parameter estimation, C_1 parameter must also be identified. In [4] following α estimation from the energy-based CF, an additional geometric CF was used for assessing C_1. In this work, an alternative method is applied, where the principle of virtual work ($\delta W_{int} = \delta W_{ext}$) is used for the estimation of C_1 according to Eq. (12). ${C_1}^f$ denotes the assumed C_1 value in Eq. (11) for the estimation of f (${C_1}^f$=1000 Pa) This method was applied to the original 3D data set, and was able to approximate the GT value (C_1=989 Pa).

$$C_{1\,sol} = \frac{\delta W_{ext}}{\left(\frac{\delta W_{int}}{{C_1}^f} \right)} \tag{12}$$

3 Results

The estimated parameters are reported in Table 1, together with the L^2 norm of error in deformation. The impact of parameter errors in the stress-strain curve is illustrated in Fig. 3. Note that the choice of other coupled parameters (taking α =10 or α = 50) lead to a small error in deformation but to a large error in the strain-stress relationship.

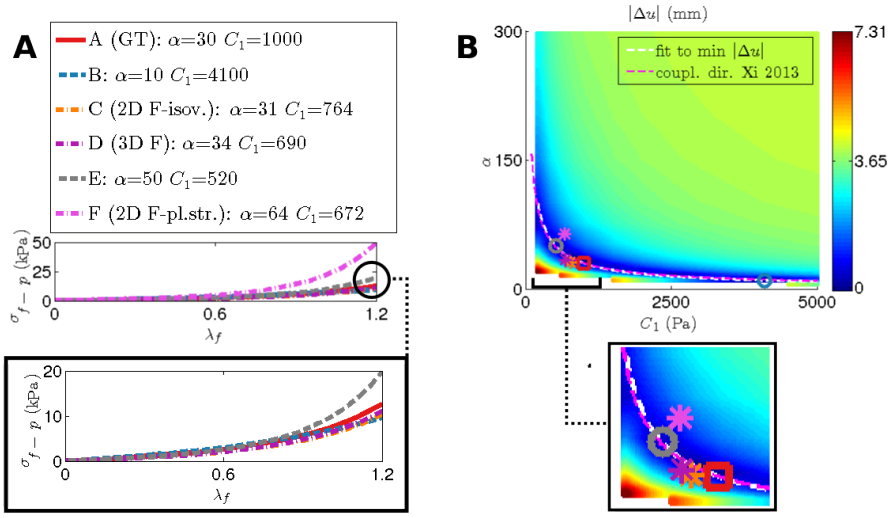

Fig. 3. A. Impact of parameter errors in the stress-strain relationship by comparison of the six parameter sets (ground truth, estimated parameters from the 2D analysis and two coupled sets of parameters- see also Sec. 2.4 and Table 1). Note that the mean and maximum stretch ratio along the fiber direction (λ_f) in the original 3D data set of Sec. 2.2 is 1.09 and 1.17 respectively. **B**. The position in paremeter space of the ground truth (marked as square), the identified parameters from 3D and 2D deformation data (marked as asterisks) and the 'coupled' parameters at $\pm$ 20 α_{GT} (marked as circles) with respect to the coupled parameter line (See Sec. 2.4).

The cumulative results from the processing of both data sets (availability of 3D deformation vs. 2D deformation) and both analysis strategies (plane strain vs. isovolumic) are shown in Table 2.

4 Discussion

This study provides the initial evidence of the feasibility of the unique material parameter estimation of a transversely isotropic material model from 2D long axis images. The proposed strategy uses a CF based on energy conservation [4] that addresses the problem of parameter coupling in myocardial material laws [6,

Table 1. Estimated parameters by the three alternative combinations of data an assumptions, together with their $|\Delta \boldsymbol{u}|$ residual. For reference, the residual with two alternative ('coupled') sets of parameters is provided (see also Sec. 2.4 and Fig. 3).

	Estimated parameters			Coupled parameters	
	3D F	**2D F-pl.str.**	**2D F-isovol.**	**-20 α_{GT}**	**+20 α_{GT}**
α	34	64	31	10	50
C_1	690	672	764	4100	50
$\|\Delta \boldsymbol{u}\|$ (mm)	0.54	1.57	0.65	0.26	0.33

3]. In this contribution a modified version of this method based on the expression of virtual work was employed and extended, not only to cope with the lack of 3D data, but to also allow the estimation of the complete set of parameters without the need of mechanical simulations.

Two different types of synthetic long axis data sets were tested against this framework: one which includes the 3D deformation of the myocardium along the imaging plane (Case 1) and one where only 2D deformation is available (Case 2). For the second data set two different assumptions regarding the out-of-plane deformation of the myocardium (plane strain and isovolumetric deformation) were tested. The results showed that the exponential α parameter was sufficiently identified in the case of 3D deformation data availability, and, in the absence of out-of-plane deformation, when the incompressibility assumption was used to approximate part of the unknown deformation gradient terms. In both these cases the errors were small and not proportional to the α value (compare the two GT models: α=30, C_1=1000Pa vs. α=100, C_1=300Pa in Table 2). Conversely, the plane strain assumption did not perform well. The superior performance of the isovolumic assumption is due to its better approximation of the 'real' 3D data deformation field. Specifically, the deformation gradient from the isovolumic assumption matched better to the original 3D deformation gradient provided by the first data set, as the shear out-of-plane components ($\partial y/\partial X$, $\partial y/\partial Z$, $\partial x/\partial Y$, $\partial z/\partial Y$) were small (in the order of 10^{-3}-10^{-2}), while the mean $\partial y/\partial Y$ component is about 1.10. Therefore assuming ($\partial y/\partial Y$)=1 according to the plane strain assumption creates an error of at least an order of magnitude bigger comparing to the error introduced by neglecting the off-plane shear terms which occurs in both plane strain and isovolumetric assumptions.

In the recovery of the full set of parameters, errors were larger for estimating C_1, as it is affected by any error in the estimated α paremeter (Eq. (12)). However, these errors did not lead to large discrepancies in the resulting stresses, where there was good aggreement with the behaviour of the GT α-C_1 pair (see Fig. 3). Moreover, a comparison of the global displacement error $|\Delta \boldsymbol{u}|$ from forward simulations of the original 3D model (Sec. 2.2) with the identified parameters to simulations with parameter sets that lie on the 'principal' coupling line [6] demonstrates the good performace of the identified parameters in terms of deformation prediction (Table 1). On the contrary, not addressing the param-

Table 2. Default and sensitivity analysis results for all data sets (see Sec. 2.2, 2.4).

Data set / analysis:		3D $\boldsymbol{F}$		2D $\boldsymbol{F}$: Plane str.		2D $\boldsymbol{F}$: Isovol.	
GT	Change to GT	α_{sol}	C_{1sol} (Pa)	α_{sol}	C_{1sol} (Pa)	α_{sol}	C_{1sol} (Pa)
α=30 C_1=1000[a]	None	34	690	64	672	31	764
	Pressure:						
	+10% $\bar{p_C}$ offset	31	832	59	801	29	885
	-10% $\bar{p_C}$ offset	36	600	68	580	34	629
	$\boldsymbol{F}$ noise:						
	STD 1% $\bar{F}_{ij}$	19	1522	108	258	86	103
	STD 2% $\bar{F}_{ij}$	9	3600	73	520	162	7
	Fibers: $\pm$ 90 ^{o}	33	752	49	832	32	773
	(r_f,r_{ft},r_t)=						
	(0.85,0.1,0.05)	32	1052	69	1810	29	1018
	(0.34,0.33,0.33)	30	647	50	543	30	649
α=100 C_1=300 [b]	None	104	215	176	235	95	239
r_f=0.85 [c]	Fibers: $\pm$ 90 ^{o}	24	1180	28	1518	24	1111

Material parameters used in each GT data set: [a]. C_1= 1000, α=30, r_f=0.55, r_{ft}=0.25, r_t=0.2. [b]. C_1= 300, α=100, r_f=0.55, r_{ft}=0.25, r_t=0.2. [c]. C_1=1000 Pa, α=30, r_f=0.85, r_{ft}=0.1, r_t=0.05. (see also Sec. 2.2)

eter coupling problem can lead to an error in the predicted developing stresses within the range of cardiac deformation (Fig. 3) [4].

The sensitivity analysis showed that the biggest source of error in parameters was the noise in the deformation field, which is an anticipated result given the exponential nature of the material law and the formulation of the proposed CF (Eq. (11)) with the additional term $\boldsymbol{E} : D\boldsymbol{E}[\delta\boldsymbol{u}]$ compared to the previously proposed energy based CF [4]. However, this result does not discredit the proposed methodology, as the type of white Gaussian noise is unrealistic (it is common practice that image derived deformation data are regularised [13]) and was used only in lack of a more suitable approach to model real image registration noise. The effect of pressure offsets in the data, altered fiber field and prescribed anisotropy parameter ratios in the model on the estimated α values was small and comparable to the 3D data analysis results [4], although a higher sensitivity to the fiber field in the case of a highly anisotropic myocardium should be noted (last row of Table 2).

In this work we have examined the feasibility of parameter estimation from 2D imaging data in a synthetic data set, where the use of a perfect symmetric long axis plane promote a good performance of our proposed parameter estimation strategies. However, the benefit of symmetry is lost in real data and additional information may be required for estimating parameters from clinical

images. Moreover, the good performance of the analysis with the isovolumic assumption may not hold when processing real cardiac images, as a higher amount of out-of-plane shear components (such as torsion) is expected and also the assumption of incompressibility can be challenged due to the changes in myocardial volume caused by perfusion.

Further work is required to investigate the possibility of reducing parameter errors (especially in the C_1 material parameter) and the feasibility of this approach with clinical data, addressing the challenges in modelling real cardiac data [6, 8, 4], and to define the optimal strategy combining data acquisition and model analysis.

5 Conclusions

This study provides preliminary in-silico evidence of the feasibility to provide a unique parameter estimation with tolerable errors from a partial 2D observation of the 3D anatomy.

References

1. D. Burkhoff, "Mortality in heart failure with preserved ejection fraction: an unacceptably high rate," *European Heart Journal*, vol. 33, no. 14, pp. 1718–1720, 2012.
2. D. Westermann, M. Kasner, P. Steendijk, F. Spillmann, A. Riad, K. Weitmann, W. Hoffmann, W. Poller, M. Pauschinger, H.-P. Schultheiss, and C. Tschöpe, "Role of left ventricular stiffness in heart failure with normal ejection fraction.," *Circulation*, vol. 117, no. 16, pp. 2051–60, 2008.
3. H. Gao, W. G. Li, L. Cai, C. Berry, and X. Y. Luo, "Parameter estimation in a Holzapfel–Ogden law for healthy myocardium," *J Eng Math*, vol. 95, no. 1, pp. 231–48, 2015.
4. A. Nasopoulou, A. Shetty, J. Lee, D. Nordsletten, C. A. Rinaldi, P. Lamata, and S. Niederer, "Improved identifiability of myocardial material parameters by an energy-based cost function," *Biomechanics and Modeling in Mechanobiology*, 2017.
5. J. M. Guccione, A. D. McCulloch, and L. K. Waldman, "Passive material properties of intact ventricular myocardium determined from a cylindrical model.," *Journal of biomechanical engineering*, vol. 113, no. 1, pp. 42–55, 1991.
6. J. Xi, P. Lamata, S. Niederer, S. Land, W. Shi, X. Zhuang, S. Ourselin, S. G. Duckett, A. K. Shetty, C. A. Rinaldi, D. Rueckert, R. Razavi, and N. P. Smith, "The estimation of patient-specific cardiac diastolic functions from clinical measurements.," *Med Image Anal*, vol. 17, no. 2, pp. 133–46, 2013.
7. D. D. Streeter, H. M. Spotnitz, D. P. Patel, J. Ross, and E. H. Sonnenblick, "Fiber orientation in the canine left ventricle during diastole and systole.," *Circ Res*, vol. 24, no. 3, pp. 339–47, 1969.
8. M. Hadjicharalambous, R. Chabiniok, L. Asner, E. Sammut, J. Wong, G. Carr-White, J. Lee, R. Razavi, N. Smith, and D. Nordsletten, "Analysis of passive cardiac constitutive laws for parameter estimation using 3D tagged MRI," *Biomechanics and Modeling in Mechanobiology*, vol. 14, no. 4, pp. 807–828, 2014.

9. J. Lee, A. Cookson, I. Roy, E. Kerfoot, L. Asner, G. Vigueras, T. Sochi, S. Deparis, C. Michler, N. P. Smith, and D. A. Nordsletten, "Multiphysics Computational Modeling in CHeart," *SIAM J Sci Comput*, vol. 38, no. 3, pp. C150–78, 2016.
10. M. Hadjicharalambous, J. Lee, N. P. Smith, and D. A. Nordsletten, "A displacement-based finite element formulation for incompressible and nearly-incompressible cardiac mechanics.," *Comput Methods Appl Mech Eng*, vol. 274, no. 100, pp. 213–236, 2014.
11. O. Zienkiewicz, R. Taylor, and J. Zhu, *The Finite Element Method: its Basis and Fundamentals*. Elsevier, 2010.
12. J. Bonet and R. D. Wood, *Nonlinear Continuum Mechanics for Finite Element Analysis*. Cambridge University Press, second ed., 2008.
13. D. Rueckert, L. I. Sonoda, C. Hayes, D. L. Hill, M. O. Leach, and D. J. Hawkes, "Nonrigid registration using free-form deformations: application to breast MR images.," *IEEE transactions on medical imaging*, vol. 18, no. 8, pp. 712–21, 1999.